

Prospects for a Higgs discovery in the channel $H \rightarrow WW \rightarrow l\nu l\nu$ with no hard jets

Bruce Mellado, William Quayle, Sau Lan Wu

University of Wisconsin - Madison
Department of Physics

Abstract

We analyze the potential for a Higgs discovery in the channel $H \rightarrow WW \rightarrow l\nu l\nu$, where the Higgs is produced in events that survive a full jet veto. Control samples for the dominant backgrounds are presented, and systematic errors are discussed. The most important systematic error in this analysis is the theoretical uncertainty on the shape of the dilepton opening angle in the transverse plane; we find that this uncertainty is approximately 5%. We present results based on full simulation of the major signal and background processes, and discuss future work necessary to fully prepare for data-taking. We demonstrate that, for a 160 GeV Higgs mass, a 5σ significance can be achieved with less than about 2 fb^{-1} of integrated luminosity.

1 Introduction

The search for the Higgs boson called for by the Standard Model is arguably one of the most important topics in high-energy particle physics today. [1, 2, 3, 4, 5, 6] For a very broad range of masses the dominant decay mode of the Standard Model Higgs boson is the decay $H \rightarrow WW$. In this note, we study the prospects for a Higgs search in events that survive a full jet veto and both W bosons decay leptonically. The $H + 0j$ channel where $H \rightarrow WW \rightarrow l\nu l\nu$ is not new; it was proposed in [7] and studied within the context of the ATLAS detector in [8]. However, the recent availability of Monte Carlo generators like MC@NLO [9, 10], Sherpa [11], and Alpgen [12, 13, 14], which can more accurately model the transverse momentum of the WW system, prompts a reanalysis of this channel. In Section 2, we discuss the signal, the dominant backgrounds, and the Monte Carlo generators we use to model them. In Section 3 we discuss our event selection, and in Section 4 we describe the control samples we use to estimate the contributions from the two dominant backgrounds in the analysis, and we discuss the most important systematic errors. In Section 5, we demonstrate using full simulation that the performance assumed in fast simulation is reasonable, and we outline a potential strategy to determine (using data) the performance of variables related to b-tagging. Lastly, in Section 6, we discuss the sensitivity of the $H \rightarrow WW \rightarrow l\nu l\nu + 0j$ channel.

2 Signal and Background Processes

We consider the following signal and background processes:

- Higgs production via gluon-gluon fusion. This is the dominant production mechanism for the signal we are looking for; we model it with the generator provided in MC@NLO. We normalize the cross-section for the signal to the official values adopted by the ATLAS collaboration in [15].
- Higgs production via Vector Boson Fusion. Because the final state of this process is typically a Higgs associated with two hard jets, this signal production mechanism is strongly rejected by the jet veto; a dedicated search for Higgs production by this mechanism can be found in [16]. We model this process with the generator provided in PYTHIA. [17, 18]¹ As we did for the gluon-gluon fusion contribution, we normalize the cross-section to the official values adopted by ATLAS.
- QCD WW production. A quark and an antiquark annihilate to form two W bosons. This is the dominant background here; we model it with the generator provided in MC@NLO version 3.1. It is important to note that MC@NLO only calculates the $O(\alpha_s^0)$ and $O(\alpha_s^1)$ contributions to this process; it does not compute

¹For historical reasons, the contribution from events where either W decays to $\tau\nu_\tau$ is neglected.

the $O(\alpha_s^2)$ contribution at the level of the matrix element. Normally, one would neglect this contribution on the grounds that it is higher-order, but in this case, such an approximation turns out to be rather poor. The $O(\alpha_s^2)$ contribution to this background contains gluon-initiated diagrams that produce W pairs via a quark loop; because the gluon density of the proton is expected to be large in the kinematic region of interest, the contribution from gluon-initiated diagrams is nontrivial. Moreover, the helicity structure of the W pair in the $O(\alpha_s^2)$ contribution is not the same as for the $O(\alpha_s^0)$ and $O(\alpha_s^1)$ contributions. This is a more serious concern for this analysis than the overall normalization of the WW background, because we use the helicity structure of the W pair (and the kinematic structure that implies for the W decay products) to determine the normalization of the WW background in the signal-like region. In this note, we model the $gg \rightarrow WW$ contribution to the overall QCD WW background with the generator documented in [19]. It is worthwhile to point out that this calculation of $gg \rightarrow WW$ ignores the contribution from heavy quark loops and includes off-shell W decays. Another calculation [20] is available that includes the heavy quark loops, but we do not use this calculation because it is performed in the narrow-width approximation for the W bosons. For the calculation in [19], one would expect that while the inclusion of the heavy quark loops might have some effect on the kinematics of the W decay products, the most important effect would be an increase of the $gg \rightarrow WW$ cross-section by at most a few tens of percent. We also note that the $gg \rightarrow WW$ event generators presently available are not a complete calculation of the $O(\alpha_s^2)$ contribution to $pp \rightarrow WW$. In particular, processes such as $gg \rightarrow WWqq$ and $qq/qg \rightarrow WW$ (to order α_s^2) are not present, but are expected to be small compared to the contribution from $gg \rightarrow WW$ via a quark loop.

- $t\bar{t}$ production. Two W bosons are produced in association with two b jets. We expect that the cross-section will be dominated by doubly resonant $t\bar{t}$ production. The absolute cross-section for the contribution from single top production is presently only known with leading-order uncertainties, but since we normalize the top background in this analysis using data, we need only concern ourselves with its potential impact on the extrapolation from the b -tagged to the b -vetoed region. (See Section 4.1.) In any case, this background is strongly rejected by the jet veto, and can be further reduced by b -tagging cuts. In our estimation of the sensitivity of the channel under study, we use the generator provided in MC@NLO to model this background; to estimate the importance of the contribution from single-top production we use MadEvent. [21, 22, 23]
- Electroweak WW production. A W pair is produced in t -channel quark scattering. This is a minor background included for completeness; its already small cross-section is strongly reduced by the jet veto cut.²
- QCD Z/γ production. In the ee and $\mu\mu$ channels, the direct decays of $Z \rightarrow ee$

²Ibid.

and $Z \rightarrow \mu\mu$ dominate, but this background can also contribute to the $e\mu$ channel when the Z decays to a pair of τ leptons which both decay leptonically. Because of its large cross-section, this background cannot be ignored, although it is easily rejected with cuts on the leptons and missing P_T . We model this background with the generator provided in MC@NLO.³

- W+n jets production, with $n \leq 4$. This background is easily reducible at LHC due to the strong rejection ($O(10^5)$) against jets faking leptons. We model this background with Alpgen version 2.0.4, using the MLM matching prescription to merge the different jet multiplicities. Details of our treatment of the detector response to this background are outlined in Section 3.1.
- Wbb+n jets production, with $n \leq 2$. Here, the dominant contribution comes from events where one of the b jets decays semileptonically. We model these events using Alpgen, and we apply the MLM matching option provided in this version of Alpgen.

We simulate the detector using the last fortran-based release of ATLFAST, and we apply the jet energy corrections in ATLFAST-B. [24]⁴ We have also studied the $gg \rightarrow H$ signal and the main background contributions in full simulation. A discussion of the Monte Carlo samples considered, as well as details about the simulation and reconstruction, will be postponed until Section 5.

2.1 Comparison of MC@NLO, Alpgen, and Sherpa

In this subsection, we check the agreement among the predictions of the QCD WW background given by MC@NLO and by tree-level jet-parton matching algorithms like the ones in Sherpa and Alpgen. We begin with a few general comments about the generators under study.

- All three generators ignore the contribution from gluon-initiated diagrams that contain a quark box. This contribution is not negligible; in practice, we treat the gluon-initiated contribution as a separate process modelled with a separate generator.

³It is worth noting that MC@NLO requires a generator-level cut on the invariant mass on the decay products of the Z boson. We use the cut $20\text{GeV} < M_{ll} < 150\text{ GeV}$, where $l = e, \mu, \tau$, so we therefore require $M_{ll} > 20\text{ GeV}$ in our event selection if the leptons have the same flavor. This takes into account the bulk of the contribution from both $Z \rightarrow ll$ and $\gamma \rightarrow ll$; events where a soft τ pair decays leptonically will be largely rejected by the trigger as the leptons from τ decays are softer than the τ leptons that produced them.

⁴We also apply a small correction to the energy of jets for which HERWIG was used for the parton showering and hadronization; the correction is given by $(1 - 5 \times 10^{-5} P_T^{jet} + 0.042)$ where the jet P_T is measured in GeV.

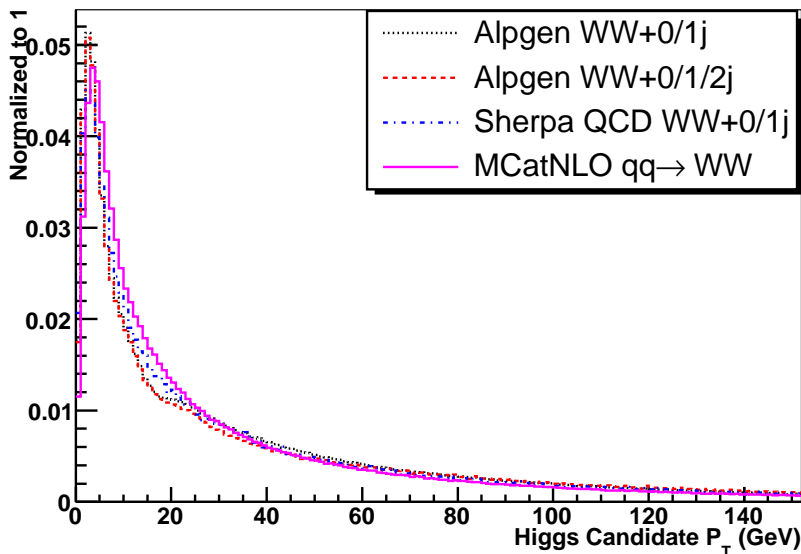


Figure 1: The transverse momentum of the Higgs candidate in QCD W pair production as given by Alpgen, Sherpa, and MC@NLO. There is a small shift in the location of the peak, but the difference is not dramatic at all.

- The matrix element calculations in MC@NLO and Alpgen were programmed by hand by their respective authors, while Sherpa uses an automated matrix element generator to write code to compute the (tree-level) matrix elements relevant to a particular process. There are therefore some differences regarding which Feynman diagrams are included in the two calculations. In the case of this analysis, where we are concerned with the production of W pairs which decay leptonically, Sherpa includes the contribution from diagrams where two Z bosons are produced, with one Z decaying to leptons and the other to neutrinos. This leads to a spike in the dilepton invariant mass distribution in events with same-flavor leptons; this feature does not appear to be present in MC@NLO and Alpgen. For this reason, we will consider only events with one electron and one muon in this section.
- MC@NLO includes the contribution from loop diagrams in its calculation; Sherpa and Alpgen rely instead on jet-parton matching schemes like the one discussed in [25].

It is worthwhile to point out that although the treatment of soft hadronic physics in Alpgen, Sherpa, and MC@NLO are all quite different, the result is nevertheless similar for the three generators. Figure 1 shows the distribution of the transverse momentum of the Higgs candidate (in the $e - \mu$ channel) given by Alpgen, Sherpa, and MC@NLO for the QCD WW background. Although a detailed study of the errors on

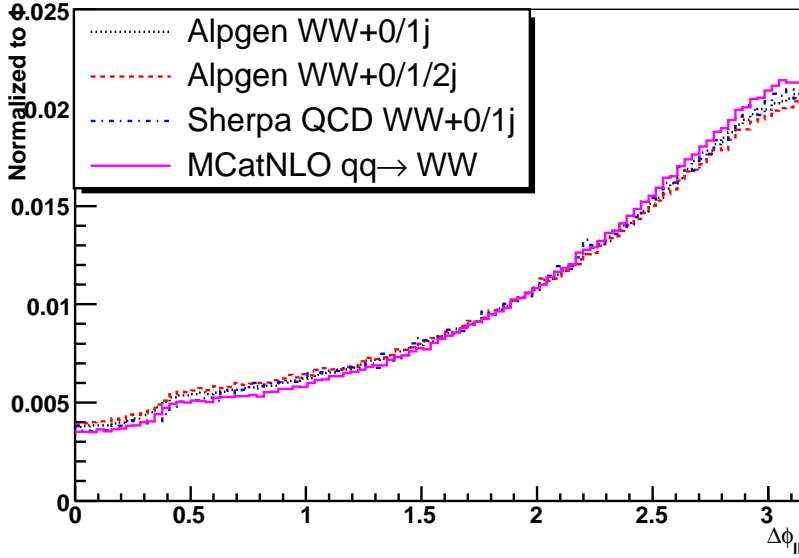


Figure 2: The distribution of the azimuthal angle between the leptons (in the $e - \mu$ channel) in QCD W pair production as given by Alpgen, Sherpa and MC@NLO.

these distributions is beyond the scope of this work, we feel that the similarity among all three generators is encouraging. We note that the Alpgen and Sherpa samples predict a slightly lower cross-section for events with Higgs candidate P_T between roughly 10 and 25 GeV. This is no doubt an artifact of the jet-parton matching method, and we expect that the behavior of this region could be tuned by tuning the matching parameters in the respective generators (although such a tuning is not necessary for our analysis).

It is also worthwhile to compare the predictions of variables related to spin correlations in the WW system, as these correlations are crucially important for the analysis. Figure 2 shows the distribution of the azimuthal angle between the leptons (in the $e - \mu$ channel) before the cuts in the next section; there is a slight difference in the shape of these inclusive distributions. The discrepancy is not serious at all; we believe it is a kinematic effect caused by the depletion in events with Higgs P_T between 10 and 25 GeV mentioned in the previous paragraph. Figure 3 shows the distribution of the dilepton opening angle in the transverse plane after all but the last three cuts of Section 3 have been applied; there is good agreement for this distribution among the various generators. Figure 4 shows the dilepton invariant mass for events with one electron and one muon (before the cuts of the analysis are applied); it is clear from the figure that the distribution of this variable is also very similar in all three generators.

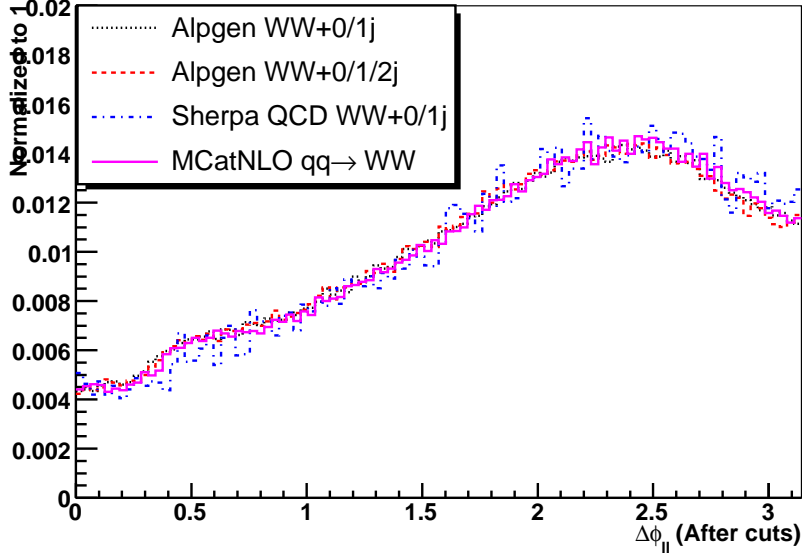


Figure 3: The distribution of the azimuthal angle between the leptons (in the $e - \mu$ channel) in QCD W pair production as given by Alpgen, Sherpa and MC@NLO. This figure plots the distributions after all cuts except the cuts on M_{ll} , $\Delta\phi_{ll}$, and M_T .

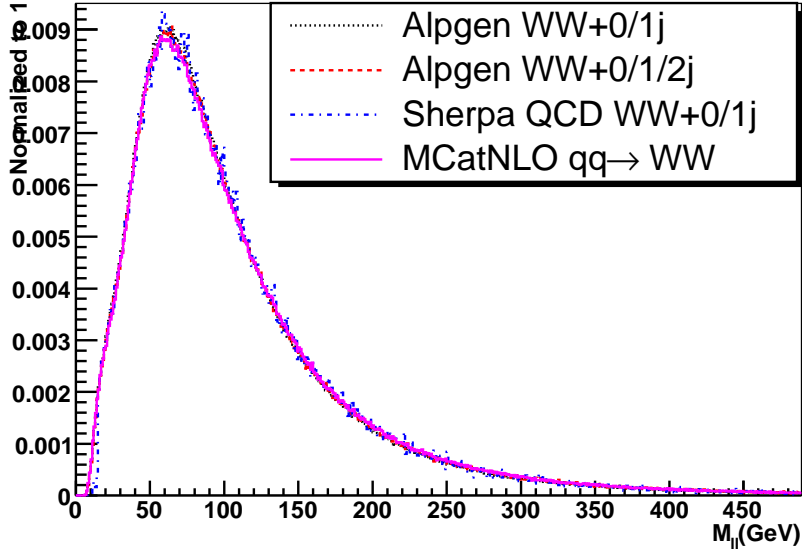


Figure 4: The distribution of the dilepton invariant mass (in the $e - \mu$ channel) in QCD W pair production as given by Alpgen, Sherpa and MC@NLO.

Cut	$gg \rightarrow H$	VBF	$t\bar{t}$	EW WW	$gg \rightarrow WW$	$qq \rightarrow WW$	Z/γ^*
Trigger	246	29.9	9698	17.0	61.4	1225	7099
P_T^{miss}	190	26.0	8143	12.0	50.3	823	634
τ Rej.	185	25.1	7586	11.4	48.5	792	151
Jet Veto	90.0	1.48	51.6	0.16	21.2	451	31.4
B Veto	89.6	1.46	37.6	0.16	21.1	449	30.8
P_T^{Higgs}	53.2	1.23	33.0	0.09	13.1	177	23.6
M_{ll}	42.9	1.10	7.85	0.02	6.31	65.2	22.0
$\Delta\phi_{ll}$	33.1	0.93	5.23	0.02	5.14	42.8	0.07
M_T	31.2	0.86	3.64	0.01	3.61	36.8	0.06

Table 1: Cut flows (in fb) for $M_H = 160$ GeV in the $e\mu$ channel.

3 Event Selection

Our event selection consists of a few basic cuts to select W pairs and several additional cuts. We begin with the following cuts:

- Trigger and Topology cuts. We require that the event has exactly two leptons with transverse momentum greater than 15 GeV in the region with $|\eta| < 2.5$. This ensures that the event passes the double-lepton trigger at ATLAS. When using fast simulation, we apply a lepton identification efficiency of 90% for each lepton.
- In order to suppress nonresonant and singly resonant $t\bar{t}$ backgrounds, we require $M_{ll} < 300\text{GeV}$. (See Section 4.1.)
- Missing Transverse Momentum. In order to reduce the large backgrounds from $Z \rightarrow ll$ decays, as well as backgrounds arising from continuum b-quark production, we require a large missing transverse momentum $\cancel{P}_T > 30\text{GeV}$. This threshold is raised to 40 GeV if the two leptons have the same flavor.
- $Z \rightarrow ll$ rejection. We reject the event if the two leptons have the same flavor and their invariant mass, M_{ll} , is between 82 and 98 GeV.
- Real τ rejection. There is a nontrivial background from the decay $Z \rightarrow \tau\tau \rightarrow ll + \cancel{P}_T$. Typically, in such decays, the neutrinos from the decays of the τ leptons are collinear with the corresponding visible leptons because the mass of the Z is so much larger than the mass of the τ . Using this approximation, we can calculate x_τ^1 and x_τ^2 , the energy fractions carried by the visible decay products of the τ leptons, and $M_{\tau\tau}$, the invariant mass of the two τ leptons. We reject the event if $x_\tau^1 > 0$, $x_\tau^2 > 0$, and $|M_{\tau\tau} - M_Z| < 25\text{GeV}$.

M_H	$M_{ll}^{min}(\text{GeV})$	$M_{ll}^{max}(\text{GeV})$	$P_T^{min}[Higgs](\text{GeV})$
130	3.1	43.8	8.0
160	6.3	64.1	11.1
200	10.6	109.9	15.2

Table 2: The upper and lower bounds on the dilepton invariant mass and the minimum transverse momentum of the Higgs candidate for three different Higgs masses.

- Hard Jet Veto. We reject the event if there are any jets with $P_T > 30\text{GeV}$ anywhere in the detector.
- Displaced vertex (b-jet) veto: we reject the event if it contains any b-tagged jets with $P_T > 20\text{GeV}$ and $|\eta| < 2.5$. In the fast simulation, we assume a b-tagging efficiency of 60% with rejections of 10 and 100 against jets from c quarks and light jets, respectively.

Our event selection is further refined by the following cuts:

- Transverse momentum of the Higgs candidate. Since the P_T distribution of the Higgs candidate tends to be small in the QCD WW background (at least for the quark-initiated portion of it), we require that $P_T[Higgs] > P_T^{min}[Higgs]$ in Table 2.⁵ This cut is one of the largest conceptual differences between this study and the one in the TDR; it was omitted there because the transverse momentum of the Higgs was not modelled well in the Monte Carlo available at the time.
- Lepton-lepton invariant mass. We require that $M_{ll}^{min} < M_{ll} < M_{ll}^{max}$, where M_{ll}^{min} and M_{ll}^{max} are given in Table 2.⁶
- Azimuthal angle between the leptons. We require $\Delta\phi_{ll} < 1.5$ radians.
- Transverse Mass. We require that $50 < M_T < M_H + 10 \text{ GeV}$.

The cross-sections after successive cuts for a representative Higgs mass of 160 GeV in the $e\mu$ channel are shown in Table 1; results for all Higgs masses are shown in Tables 12, 13, and 14 in Appendix A.

It has not escaped our attention that our cut on the transverse momentum of the WW system may be somewhat dangerous to apply; since we do not have a full

⁵The exact values of the cuts we use for various Higgs masses are given by $P_T^{min}[Higgs] = 0.103534M_H - 5.50246 \text{ GeV}$, where M_H is the Higgs mass hypothesis in GeV. To determine this parameterization, we used a Genetic Algorithm to optimize cuts for each of the Higgs masses we consider in this note, and we fit the optimal cut values with a straight line. For details on this technique, see [16].

⁶The parameterizations of the cuts we use are given by $M_{ll}^{min} = 0.108368M_H - 11.034 \text{ GeV}$ and $M_{ll}^{max} = 95.4742 - 1.26987M_H + 0.0067109M_H^2 \text{ GeV}$, where M_H is again the Higgs mass hypothesis in GeV.

calculation of $gg \rightarrow WW + 1j$, the P_T of the WW system is probably not modelled accurately in gluon-initiated QCD WW events. Rather, it is generated exclusively by Herwig's parton shower, so we need to consider the possibility that the efficiency of the P_T^{Higgs} cut we observe in $gg \rightarrow WW$ is not correct. The most extreme scenario one can define is that in a full $O(\alpha_s^3)$ calculation, all $gg \rightarrow WW$ events might pass our cut on the transverse momentum of the WW system. Dividing out the efficiency of the P_T^{Higgs} cut (about 62%) by hand suggests that this would cause the $gg \rightarrow WW$ contribution increase to about 5.6 fb, roughly 16% of the total QCD WW background cross-section. This means a total increase of 5% in the QCD WW background in the signal-like region. Now, in this analysis, we determine the background normalization from a control sample; see Section 4 for details. A quick look ahead to the results of that section (in particular, Table 4) suggests that dividing out the same 62% efficiency from the $gg \rightarrow WW$ contribution there would increase the QCD WW cross-section in the control sample by about 3%. This implies that our measurement of the QCD WW background in the signal-like region would be incorrect by at most a 2-3% as a result of our treatment of the P_T of the WW system in $gg \rightarrow WW$. This figure is small in comparison to the uncertainty calculated in Section 4.1. Moreover, it is hard to believe that the efficiency of our cut on the Higgs P_T could be so poorly predicted by a parton shower; one could imagine that a full $O(\alpha_s^3)$ treatment of the $gg \rightarrow WW$ background might increase the survival probability from 62% to 70% or perhaps even 80%, but not 100%. Because the potential inaccuracy is so insignificant, we feel that there is no significant danger in our use of the Higgs P_T to reject the $qq/qg \rightarrow WW$ background.

3.1 Fake Backgrounds

In this section, we discuss the contribution from reducible backgrounds, which are neglected elsewhere in this note. We have considered two such backgrounds: $W + jets$ and $Wbb + jets$.⁷ We model both these processes with Alpgen. The W +light jets background is heavily suppressed by the excellent rejection against fake leptons provided by the ATLAS detector. (In this note, we assume a rejection of 10^5 against jets faking leptons.) To simulate a jet faking a lepton, we use a fairly crude model in the fast simulation: out of all the jets in the event that lie within $|\eta| < 2.5$ and have $P_T > 15$ GeV, we randomly select one (there must be at least one) and randomly assign it a lepton flavor (e or μ). Then the analysis cuts are applied, assuming an event weight of 10^{-5} , and the cross-section is computed. For the $Wbb + jets$ background, the dominant contribution comes from events where there is a real (soft) lepton from the decay of one of the b-quarks, so such a treatment is not necessary. The results of this exercise are summarized in Table 3. (Note that the physical cross-section is, of course, the sum of the various jet multiplicities.) Clearly, if the rejection against fakes is as good as is presently expected, the background from these processes is at the level of a few percent. However, in the early stages of data-taking, it is not hard to imagine

⁷In principle, we should also consider $Wcc + jets$, but since the contribution from the two reducible backgrounds we consider is so small, we ignore this source of background for now.

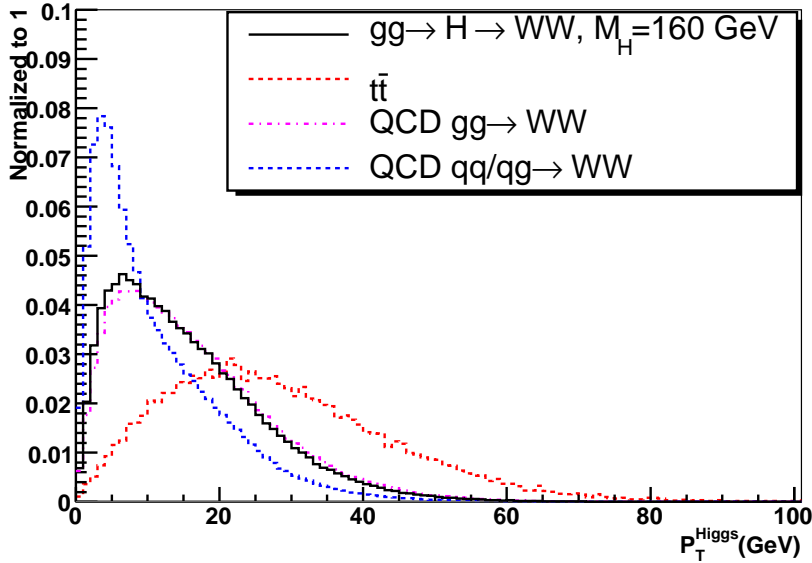


Figure 5: The distribution of the transverse momentum of the Higgs for the signal ($M_H = 160\text{GeV}$) and the two most important backgrounds. The curves are normalized to unity.

that the rejection against leptons might be smaller than the 10^5 we have assumed here. In such a scenario, it will be necessary to take the background from W +light jets into account. We expect that it will, in any case, be quite straightforward to measure the background from fakes using data: first, measure the rejection as a function of P_T and η by simply applying the lepton selection criteria to the subleading jets in a multijet event sample (assuming the leading jet is used to trigger the event), and second, apply these rejections to a set of W +jets events taken from data in a fashion similar to what we have done with Monte Carlo here.⁸ Note that since we are taking everything from data, there is no need to have a precise measurement of the lepton selection efficiency; it is enough to know the rejection. Since the contribution from fakes will be small if the ATLAS detector performs as well as it is designed to, since the uncertainty on the theoretical prediction of the $W + jets$ cross-section is large, and since the main reducible background can be measured in data with better precision anyways, we will ignore these backgrounds in the rest of this note.

⁸This approach relies heavily on the reasonable assumption that the kinematic arrangement of the jets in a $W + jets$ event is not strongly correlated to variables such as the width of the jet or the multiplicity of charged tracks within a jet. It is desirable to verify this assumption in full simulation before data-taking begins, but we consider such an undertaking to be beyond the scope of this note.

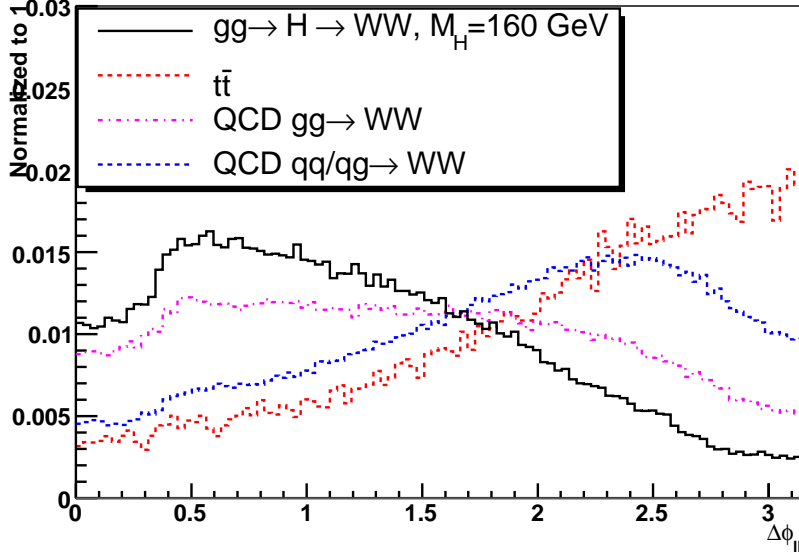


Figure 6: The distribution of the azimuthal angle (in the transverse plane) between the leptons after the application of all cuts in Section 3 except the cuts on M_{ll} , $\Delta\phi_{ll}$, and M_T .

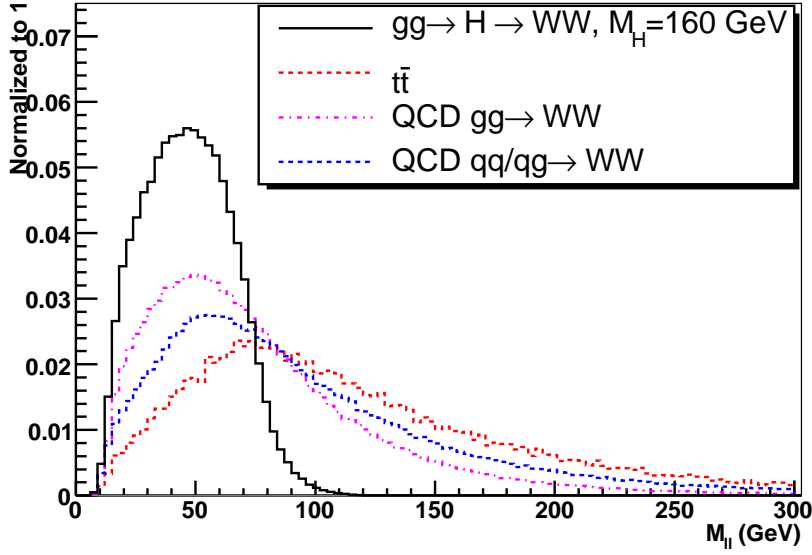


Figure 7: The distribution of the dilepton invariant mass after the application of all cuts in Section 3 except the cuts on M_{ll} , $\Delta\phi_{ll}$, and M_T .

Process	$M_H = 130\text{GeV}$	$M_H = 160\text{GeV}$	$M_H = 200\text{GeV}$
$qq \rightarrow WW$	45.02	63.20	55.97
W+0j	0.073	0.053	0.025
W+1j	0.95	0.89	0.50
W+2j	0.19	0.33	0.38
W+3j	0.014	0.023	0.029
W+4j	0.0013	0.0024	0.0031
Wbb+0j	0.41	0.44	0.36
Wbb+1j	0.072	0.10	0.10
Wbb+2j	0.023	0.023	0.020

Table 3: Cross-sections (in fb) for the fake backgrounds from W+jets for various Higgs masses. Cross-sections for W+light jets assume a 10^5 rejection against fake leptons arising from jets; cross-sections from Wbb+jets are from the set of events where at least one b-jet decays semileptonically. The cross-sections for the main irreducible background are shown for comparison.

4 Control Samples

In order to reduce the dependence of the analysis on theoretical calculations, we have defined control samples to estimate the normalization of the most important backgrounds, QCD W pair production and $t\bar{t}$ production. In this section, we describe the control samples, discuss several possible sources of systematic uncertainty, and comment on the impact of these uncertainties on the sensitivity of the analysis.

We begin by introducing the following two control samples.

- The primary control sample is adjacent to the signal-like region (discussed in Section 3), but with different cuts on the dilepton opening angle in the transverse plane, $\Delta\phi_{ll}$, and the dilepton invariant mass, M_{ll} . The event selection for the Primary control sample is the same as for the signal-like region, except that we require $\Delta\phi_{ll} > 1.5$ radians, $80 < M_{ll} < 300$ GeV, and we remove the cut on the transverse mass M_T .
- Because the Primary control sample has a large contamination from top quark events, we must introduce a b-tagged “Secondary” control sample which we will use to estimate the top quark contamination as well as the top background in the signal-like region. The cuts here are the same as in the Primary control sample, except that instead of applying a b-jet veto, we require that there be a b-tagged jet with P_T between 20 GeV and 30 GeV. In this sample, we also remove the lower bound on the dilepton invariant mass.

Table 4 shows the cross-sections in these two control samples for a representative

Sample	$gg \rightarrow H$	VBF	$t\bar{t}$	EW WW	$gg \rightarrow WW$	$qq \rightarrow WW$	$Z \rightarrow \tau\tau$
Primary	1.86	0.03	33.4	0.08	6.19	121.0	7.96
b-tagged	0.18	0.007	17.02	0.0001	0.08	1.51	1.29

Table 4: Cross-sections (in fb) in the two control samples discussed in Section 4 for $M_H = 160$ GeV, summed over lepton flavor.

Higgs mass hypothesis of 160 GeV; the cross-sections obtained for other values of the Higgs mass hypothesis are given in Tables 15 and 16 in Appendix A.

In order to make meaningful estimates of systematic errors, it is necessary to specify formally our signal extraction procedure. Once this is done, we can then define what we mean by ‘systematic errors’ in the context of our analysis. To this end, we will define three quantities:

- $\alpha_{WW} = \sigma_{WW}^{signal-like} / \sigma_{WW}^{control}$: The ratio of the QCD WW cross-section in the signal-like region over the QCD WW cross-section in the Primary control sample.
- $\alpha_{t\bar{t}} = \sigma_{t\bar{t}}^{signal-like} / \sigma_{t\bar{t}}^{b-tagged}$: The ratio of the $t\bar{t}$ cross-section in the signal-like region over the $t\bar{t}$ cross-section in the b-tagged control sample.
- $\alpha_{t\bar{t}}^{WW} = \sigma_{t\bar{t}}^{control} / \sigma_{t\bar{t}}^{b-tagged}$: The ratio of the $t\bar{t}$ cross-section in the Primary control sample over the $t\bar{t}$ cross-section in the b-tagged control sample.

The signal extraction procedure can now be explicitly written down in terms of these quantities. For the purposes of the discussion in this section, we will take their values from Monte Carlo. To determine the background in the signal-like region, first measure N_P , the number of events in the Primary control sample, and N_B , the number of events in the b-tagged control sample. Because the b-tagged control sample is comprised almost entirely of $t\bar{t}$ events, we can say, to a good approximation, that the number of $t\bar{t}$ events expected in the signal-like region is $\alpha_{t\bar{t}} N_B$.

We would like to make a similar estimate of the QCD WW background using N_P and α_{WW} , but a quick look at the cross-sections presented above indicates that there is a substantial amount of contamination from the $t\bar{t}$ background in the main control sample. We can estimate the number of $t\bar{t}$ events in the main control sample as $\alpha_{t\bar{t}}^{WW} N_B$; a good estimate of the number of QCD WW events in the main control sample is then

$$N_{WW} = N_P - \alpha_{t\bar{t}}^{WW} N_B - \text{other backgrounds.} \quad (1)$$

where the “other backgrounds” consist mainly of Drell-Yan production. With our knowledge of N_{WW} , we can now write the expected number of QCD WW events in the signal-like region as $N_{WW}^{bg} = \alpha_{WW} N_{WW}$.

M_H	α_{WW}	Raised Jet E.	Lowered Jet E.	P_T^{miss}
130	0.3976	+1.40%	-1.12%	+0.94%
160	1.0422	+1.15%	-1.04%	-0.20%
200	1.6297	+0.93%	-0.47%	+0.08%
M_H	α_{tt}	Raised Jet E.	Lowered Jet E.	P_T^{miss}
130	0.1683	+5.89%	-7.54%	-2.79%
160	0.3735	+6.88%	-7.44%	-0.08%
200	0.5917	+10.34%	-4.78%	+0.94%
M_H	α_{tt}^{WW}	Raised Jet E.	Lowered Jet E.	P_T^{miss}
130	2.0119	+9.02%	-8.99%	+0.83%
160	1.9667	+7.16%	-8.62%	+1.36%
200	1.9101	+9.75%	-8.49%	+1.33%

Table 5: The extrapolation coefficients for three different values of the Higgs mass hypothesis (Higgs masses given in GeV) and the deviation from the central value when various systematic changes are applied.

In principle, we should construct another secondary control sample out of dilepton events on the Z resonance and use it to control the Drell-Yan contribution as we did for $t\bar{t}$, but in this study we forgo such an exercise. The inclusive Drell-Yan cross-section is very large and it is likely that the relevant systematic errors will be small. Other sources of contamination in the main control sample are small enough that errors on their determination can be completely ignored. In this analysis, we therefore ignore errors arising from the subtraction of backgrounds other than $t\bar{t}$ from the main control sample.

With the above definitions, the background uncertainty in the signal-like region can be determined by a straightforward exercise in the propagation of errors; taking systematic errors into account is simply a matter of estimating the deviation in α_{WW} , α_{tt} , and α_{tt}^{WW} due to theoretical uncertainties and instrumental effects. In this analysis, there are four main sources of systematic error: uncertainties in the jet energy scale calibration, uncertainties in the missing P_T resolution, theoretical uncertainties, and the uncertainty in the b-tagging efficiency.

To estimate the jet energy scale uncertainty, we simultaneously simultaneously raise the energy scale of jets by 5% in the region with $|\eta| < 2.5$ and by 10% in the forward region. We recalculate the cross-sections and the values of α_{WW} , α_{tt} , and α_{tt}^{WW} that we would observe with this miscalibration. We then repeat the exercise, this time lowering the energy scale of the jets by 5% and 10%. The contribution of the jet energy scale uncertainty to the total systematic error on the alphas is the larger of the two deviations from the nominal value.

The exercise we perform to estimate the systematic error due to the uncertainty

in the missing P_T is quite similar. Instead of altering the jet energy scale, we smear the x and y components of the missing P_T by 5 GeV (for a total smearing of about 7 GeV). We then recalculate the cross-sections in the signal-like region and the control samples and use these values to extract the new values of α_{WW} , α_{tt} , and α_{tt}^{WW} . The uncertainty is taken to be the deviation of the new values from the nominal ones.

Estimating the b-tagging uncertainty is more difficult; it is really only appropriate to consider such an uncertainty in full simulation. It has been shown in [26] that the b-tagging performance does not have large uncertainties if the Inner Detector alignment is well-understood; for the purposes of the fast-simulation based part of our feasibility study, we therefore neglect b-tagging uncertainties. In the very early stages of data-taking, this approximation breaks down. In a future study, we will therefore attempt to better address the impact of misalignments and other systematic effects on this analysis. In the meantime, we have performed a preliminary investigation of one possible approach to measure the b-tagging performance using data; this is discussed in Section 5.

Estimating the theoretical uncertainties is a more elaborate task; for this reason, the theoretical uncertainties are described separately in the next subsection. The results of the jet energy scale and missing P_T uncertainty studies are summarized in Table 5. In our estimate of the sensitivity of this channel, we will assume jet energy scale and missing P_T uncertainties of 1.5% and 1% respectively for α_{WW} ; 8% and 2% for α_{tt} ; and 9% and 1.5% for α_{tt}^{WW} .

4.1 Theoretical Uncertainties

In this section, we consider theoretical uncertainties in the extrapolation coefficients. In the case of α_{WW} , the theoretical error is dominated by the uncertainty in the normalization of the $gg \rightarrow WW$ (via quark box) contribution; for α_{tt} and α_{tt}^{WW} , the most important concern is whether or not singly-resonant top production behaves the same way as doubly-resonant top production does in terms of the extrapolation from b-tagged to b-vetoed event samples.

The theoretical uncertainty in the value of α_{WW} is potentially the most significant uncertainty in this analysis, as recent studies have shown that the contribution of such higher order corrections to the QCD WW background can be in excess of 30% for the cuts used in those studies. Here, we have studied this contribution using MC@NLO to model the contribution from $qq \rightarrow WW$ and $qg \rightarrow WW$. We use the event generator used in [19], interfaced to HERWIG to handle parton showering and hadronization, to model the contribution from $gg \rightarrow WW$.

We take as the systematic error the sum in quadrature of the uncertainty due to the fit error in the parton density function parameterization and the uncertainty due to the choice of Q^2 scale. To estimate the parton density function uncertainty, we have generated samples of events using the CTEQ6 [27] central value parameterization and

each of the 40 error parameterizations; the uncertainty in α_{WW} is given by equation (3) in [27]. For brevity, we will omit a complete listing of the cross-sections of the $gg \rightarrow WW$ and $qq \rightarrow WW$ contributions to the QCD WW background before and after all cuts, and simply state the result: we compute an uncertainty of 2.8% in α_{WW} due to the parton density function uncertainty given by the CTEQ6 parameterization.

To assess the uncertainty due to the choice of Q^2 scale, we have generated samples of events with the renormalization scale and the factorization scale varied by factors of 8. This is an unusually large scale variation to choose; typically, a scale uncertainty will be quoted based on a scale variation of 2 or at most 4. Our motivation for this choice is the fact that we expect the K-factor for $gg \rightarrow WW$ to be large, since the K-factor for $gg \rightarrow \gamma\gamma$ has been calculated and it is slightly less than 2. [28] We examine four choices of scale variations:

- Scale 1: $Q_{ren} \rightarrow 8Q_{ren}$, $Q_{fac} \rightarrow Q_{fac}/8$
- Scale 2: $Q_{ren} \rightarrow Q_{ren}/8$, $Q_{fac} \rightarrow 8Q_{fac}$
- Scale 3: $Q_{ren} \rightarrow 8Q_{ren}$, $Q_{fac} \rightarrow 8Q_{fac}$
- Scale 4: $Q_{ren} \rightarrow Q_{ren}/8$, $Q_{fac} \rightarrow Q_{fac}/8$

Table 6 shows the cross-sections before cuts for the $gg \rightarrow WW$ and $qq \rightarrow WW$ contributions, with the central-value Q^2 scales and the four modified scale choices. Table 7 shows the cross-sections after cuts in the signal-like region and the Primary control sample for three different choices of the Higgs mass hypothesis. The results can be summarized as follows: for $M_H = 130$ GeV, the largest variation in α_{WW} is 3.8%; for $M_H = 160$ GeV, it is 4.1%; and for $M_H = 200$ GeV, it is 6.8%. In the results we report in this note, we will assume for simplicity an M_H -independent Q^2 scale uncertainty of 4.1%. We feel that this is a reasonable approximation, since this channel is already quite weak at $M_H = 200$ GeV. The total theoretical uncertainty we assume on the prediction of α_{WW} is therefore 5%. Adding this result in quadrature with the uncertainties computed in the previous subsection, we find a total uncertainty of 5.3% on α_{WW} .

Previous studies of the $H \rightarrow WW + 0j$ channel typically included a sizeable contribution to the background from single-top production (sometimes also referred to as $pp \rightarrow Wt$). However, these estimates were generally based on single-top matrix elements which neglected the interference between single-top production and top quark pair production. At LHC, it is expected that the intrinsic b-quark content of the proton will be dwarfed by gluon splittings; therefore, the dominant contribution to the Wt final state is actually Wtb (or equivalently, $WWbb$), where one of the b-quarks is a spectator quark that ends up being soft or lost down the beam pipe. A procedure for generating both $pp \rightarrow t\bar{t}$ and $pp \rightarrow Wt$ without double-counting at leading order was presented in [29], and a calculation including off-shell effects and spin correlations in the $WWbb$ system at tree level was presented in [30].

Scale Choice	$gg \rightarrow WW$	$qq \rightarrow WW$
Central Value	487.77	11302.44
Scale 1	239.93	12862.82
Scale 2	1058.97	9076.86
Scale 3	278.17	11189.52
Scale 4	913.38	11702.80

Table 6: Cross-sections (in fb) for $gg \rightarrow WW$ and $qq \rightarrow WW$ with the 5 Q^2 scale choices considered.

M_H	sample	$gg \rightarrow WW$ Sig. Reg.	$qq \rightarrow WW$ Sig. Reg.	$gg \rightarrow WW$ Cont. Samp.	$qq \rightarrow WW$ Cont. Samp.	α_{WW}
130	Central	2.96	45.02	7.66	172.79	0.2659
	scale1	1.35	49.01	3.99	189.75	0.2599
	scale2	6.65	35.20	16.17	142.58	0.2636
	scale3	1.74	46.91	4.24	175.51	0.2707
	scale4	5.13	44.00	15.18	176.61	0.2562
160	Central	6.45	63.20	6.38	130.10	0.5103
	scale1	2.92	69.25	3.33	143.83	0.4904
	scale2	14.5	49.03	13.46	107.44	0.5255
	scale3	3.81	65.02	3.54	131.92	0.5081
	scale4	11.1	61.81	12.66	133.51	0.4988
200	Central	7.62	55.97	4.82	87.89	0.6859
	scale1	3.50	62.70	2.51	97.65	0.6609
	scale2	17.1	43.55	10.14	72.65	0.7326
	scale3	4.50	57.30	2.67	89.05	0.6738
	scale4	13.2	55.40	9.57	90.54	0.6852

Table 7: Cross-sections for the signal-like region and the Primary control sample, with the corresponding extrapolation coefficients, using the nominal assumptions and the 4 altered scale choices.

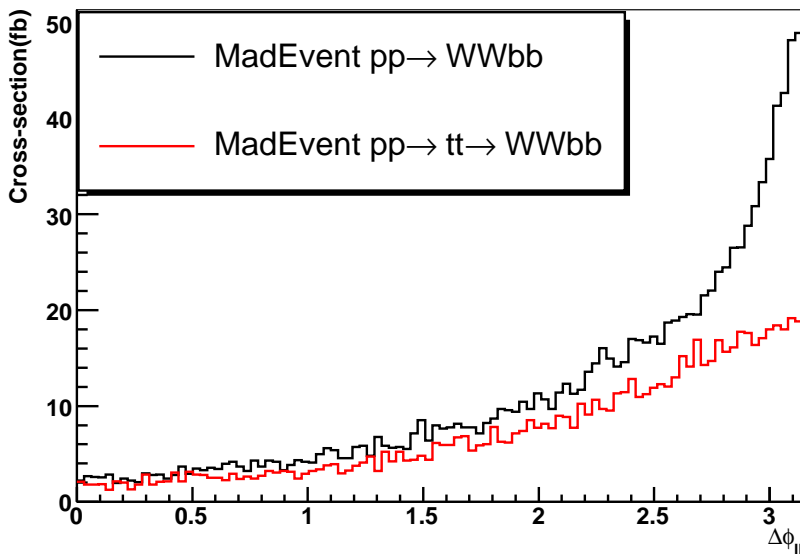


Figure 8: The dilepton opening angle in the transverse plane, after all cuts except the cuts on M_{ll} , $\Delta\phi_{ll}$, and M_T . Notably, this plot does not contain the requirement $M_{ll} < 300$ GeV.

Unfortunately, however, we know of no event generator available at the time of this writing which takes into account both the one-loop radiative corrections to $WWbb$ production and the interference between $t\bar{t}$ and Wt . Our approach to this background is therefore to consider several crude approximations and take the difference as an uncertainty. In addition to the $t\bar{t}$ Monte Carlo sample (from MC@NLO) that we have used in the other sections of this note and which we take as our default estimate of the top background, we have generated two separate $WWbb$ Monte Carlo samples using MadEvent. One includes only doubly-resonant top quark pair production, and the other includes the full $WWbb$ final state. For this generation, we have allowed the b-quarks to be generated with P_T as low as 1 GeV, and with pseudorapidity as high as 100. The divergence that occurs in the nonresonant $WWbb$ production as the spectator quark becomes soft is therefore regularized more by the b-quark mass than by our P_T cutoff. One would expect large logarithms to play an important role in such a calculation, and we therefore feel it is likely that the single-top contribution is overestimated in our nonresonant $WWbb$ Monte Carlo. This is exactly what we want if we are to prove that our analysis is robust against larger-than-expected contributions from single-top production.

We have applied the cuts from Section 3 and those from Section 4 to these two samples to assess the importance of single-top production in this analysis. First, we point out the reason for the upper bound on the dilepton mass that we use throughout

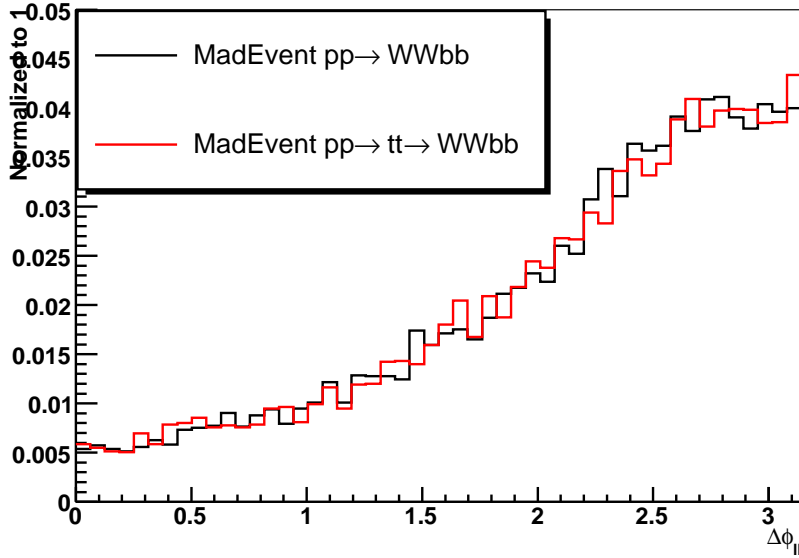


Figure 9: The dilepton opening angle in the transverse plane, after all cuts except the cuts on M_{ll} , $\Delta\phi_{ll}$, and M_T . This plot does include the requirement $M_{ll} < 300$ GeV.

this analysis ($M_{ll} < 300$ GeV): Figure 8 shows the dilepton opening angle in the $pp \rightarrow tt \rightarrow WWbb$ and $pp \rightarrow WWbb$ samples after all cuts except the cuts on M_{ll} , P_T^{Higgs} , and $\Delta\phi_{ll}$; there is a clear and striking difference in the shape of the two curves. By contrast, if we require that the dilepton mass be less than 300 GeV, we see the distributions in Figure 9. (Note that the cross-sections obtained with the two samples are still different, but the *shape* of the $\Delta\phi_{ll}$ distribution is the same in the two samples.)

Table 8 shows the $WWbb$ background cross-sections in the signal-like region, the Primary control sample, and the b-tagged control sample obtained with the leading-order doubly-resonant and fully non-resonant $WWbb$ samples. We note that the difference in the prediction of α_{tt} and α_{tt}^{WW} are approximately 9% for α_{tt} and approximately 10% for α_{tt}^{WW} . We again take these uncertainties to be uncorrelated with the ones computed in the previous section, and we arrive at total uncertainties of 12.2% for α_{tt} and 13.5% for α_{tt}^{WW} . It is not clear that these values of the uncertainty will remain unchanged for the full simulation; it stands to reason that the theoretical uncertainty we have assumed is a function of both the b-tagging efficiency and its dependence on the b-quark P_T . In Section 5 we will discuss a potential method to extract from data the probability to find a b-tagged jet in the jet-vetoed region.

M_H	Process	Signal-like	Cont. Samp.	b-tagged	α_{tt}	α_{tt}^{WW}
130	$WWbb$	6.14	120.28	49.85	0.1232	2.4129
130	$tt \rightarrow WWbb$	4.54	87.36	40.03	0.1135	2.1826
160	$WWbb$	13.34	109.41	47.13	0.2829	2.3211
160	$tt \rightarrow WWbb$	9.80	80.77	37.72	0.2599	2.1413
200	$WWbb$	19.72	93.76	42.88	0.4599	2.1863
200	$tt \rightarrow WWbb$	15.01	71.07	34.91	0.4302	2.0357

Table 8: Cross-sections (in fb) and extrapolation coefficients for the $t\bar{t}b\bar{b}$ background for various masses, using MadGraph to model the $WWbb$ background.

5 Full Simulation Studies

In order to show that our fast-simulation based results are reasonable, and to shed light on possible avenues for future work, we have performed some limited studies based on fully simulated events. To be clear, we should point out from the start that the work presented in this section falls short of a complete and detailed analysis of the $H \rightarrow WW$ channel in full simulation; a full treatment, especially of systematic errors studyable only in full simulation (such as misalignment effects, etc.), is beyond the scope of this work and will be addressed in a future study. Here, our main purpose is to show that the performance we have assumed in the fast simulation study is achievable in full simulation. In particular, it is not obvious that the b-tagging efficiency we assumed in fast simulation ($\epsilon_b = 60\%$ for jets with $P_T > 20$ GeV and $|\eta| < 2.5$, $\epsilon_b = 0$ otherwise) is at all reasonable in the kinematic region of interest, nor is it obvious that events where one of the leptons comes from the semileptonic decay of a b quark will be completely negligible. With that in mind, we have studied the following processes in full simulation:

- $gg \rightarrow H \rightarrow WW$, generated with (as in fast simulation) MC@NLO, simulated with Athena version 9.0.4, and reconstructed with Athena version 10.0.1
- doubly-resonant $t\bar{t}$ production, generated with MC@NLO, simulated with Athena version 9.0.4, and reconstructed with Athena version 10.0.1

These events were simulated using the “Rome” (initial) layout of the ATLAS detector. Our analysis involves the following physics objects:

- Muons. We use the muons from the MuonID package. We require that the $\text{sum}(P_T)$ of tracks in a cone of 0.2 units of R around a muon be less than 5 GeV.
- Electrons. We use the IsEM (bit 15) flag to select clusters in the electromagnetic calorimeter, and require that they have a matched track. The electron energy is given by the energy of the cluster, while its η and ϕ come from the track. We require that the $\text{sum}(P_T)$ of tracks in a cone around an electron be less than 10 GeV.
- Jets. We use cone jets with a radius of 0.4. It is worth noting that in the fast simulation, a jet calibration was applied to correct the measured jet energy to the corresponding parton energy. No such correction is applied in the full simulation, but in this analysis, such a difference only really affects the jet veto. Since jets with transverse momentum close to the jet veto threshold are corrected by a factor on the order of 1.5, we lower the jet veto threshold in full simulation to 20 GeV instead of 30 GeV.
- Tracks. We use tracks from IPatRec.

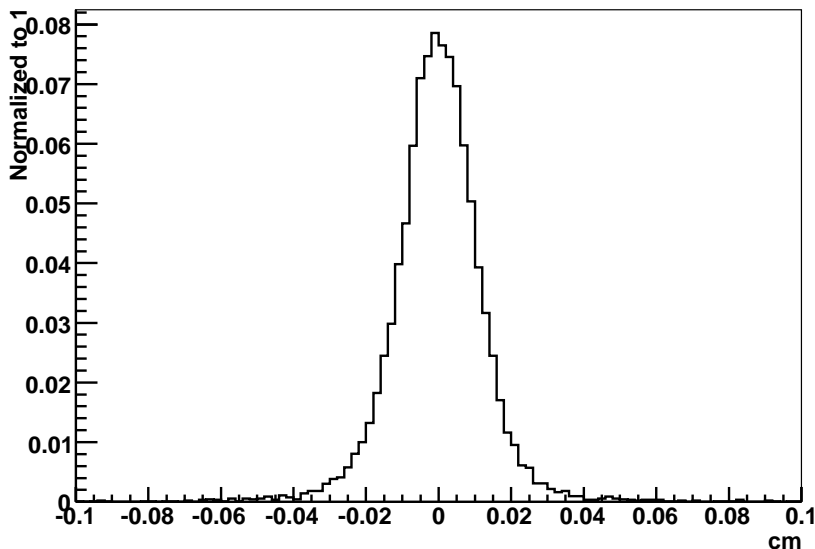


Figure 10: The z distance between the reconstructed primary vertex and the truth.

- Missing Transverse Momentum. We use the object-based missing E_T approach described in [31], with calibration constants suitable to Athena version 10.0.1.

The analysis in full simulation proceeds almost exactly as it does in fast simulation; the only material difference is the fact that in full simulation, we must be more specific than to simply say that we reject ‘b-tagged’ jets. We therefore define the following rudimentary “Top-killing” algorithm:

- We first find a primary vertex using the tracks from the two leptons in the event. We fit these tracks to a single vertex and require that the χ^2 of the fit be less than 25. The two tracks that participate in this fit are excluded from the rest of the Top-killing cuts. Figure 10 shows the distance in z between the reconstructed primary vertex and the Monte Carlo truth. The resolution in z obtained by this procedure is about $105 \mu\text{m}$, and is sufficient for our purposes. We could improve the precision of this reconstruction by including more tracks in the fit; we do not pursue this opportunity because it is simpler and because we do not wish to bias the distributions of the other Top-killing variables.
- We look for displaced vertices in a cone of 0.3 around each identified jet in the event, using the VKalVrt package [32, 33]. We select the jet that has the largest (in magnitude) displacement significance, and if that significance is positive and larger than 3σ , we veto the event. Figure 11 shows the displacement significance

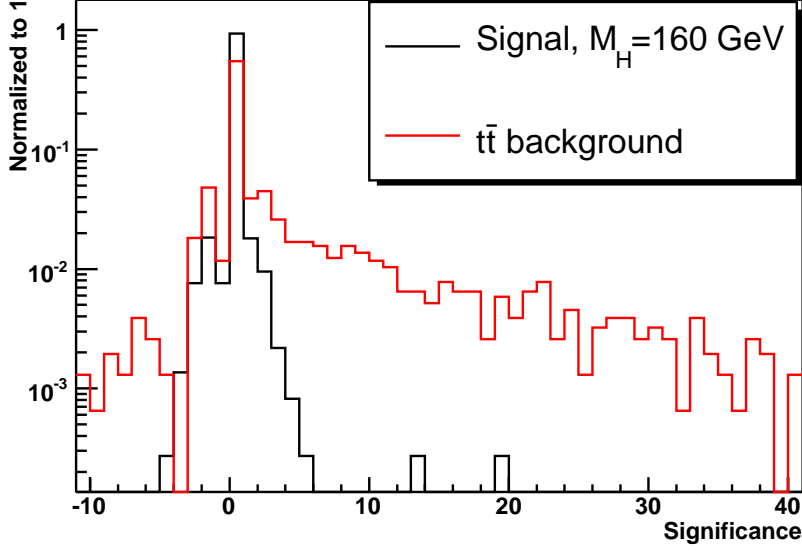


Figure 11: The normalized 3D distance between the primary vertex and the most displaced secondary vertex in the event in signal (black) and $t\bar{t}$ background (red). This plot shows the distribution after the jet veto is applied.

of the most displaced vertex in the event after the jet veto is applied; our cut gives a survival probability of roughly 70% for top events and about 98% for signal.

- We calculate the 3D impact parameter significance with respect to the primary vertex of all tracks with $P_T > 2$ GeV in a cone of 0.3 around either of the two highest- P_T jets in the event, and we take the sum. Figure 12 shows the distribution of this variable after the vertex displacement cut; if it is larger than 5, we reject the event. This cut yields a survival probability of about 70% for the $t\bar{t}$ background and about 97% for signal.
- We calculate the scalar sum of the transverse momenta of all tracks with $P_T > 2$ GeV whose 3D impact parameter significance with respect to the primary vertex is less than 1.5. Figure 13 shows the distribution of this variable after the other Top-killing cuts are applied. If this quantity is greater than 15 GeV, we reject the event. This cut is tantamount to a tightening of the jet veto, but the caveats surrounding the calibration of low- P_T hadronic depositions are not present here. In principle, it may therefore be possible to apply a much tighter cut than the one we apply here; however, because this cut is essentially a tracking-based jet veto, it is as difficult to control as the jet veto. For this reason, we only apply a loose cut for the present analysis.

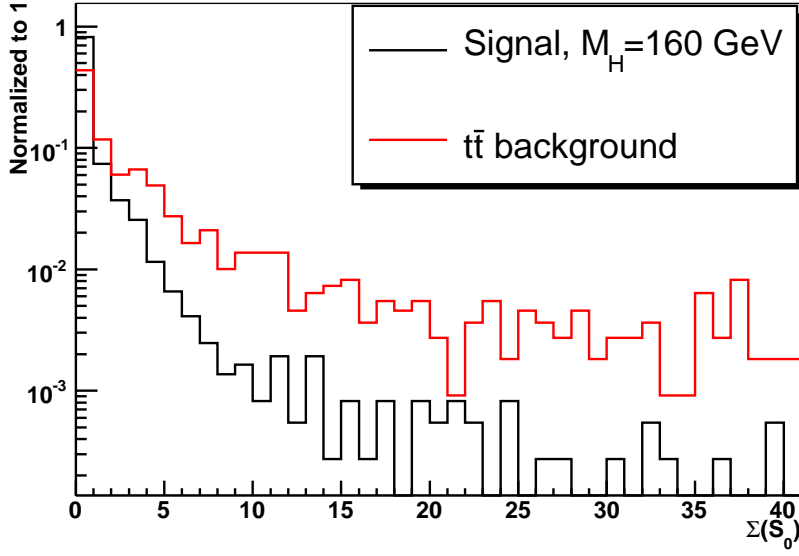


Figure 12: The sum of the 3D impact parameter significances (S_0) of all tracks near either of the two leading jets.

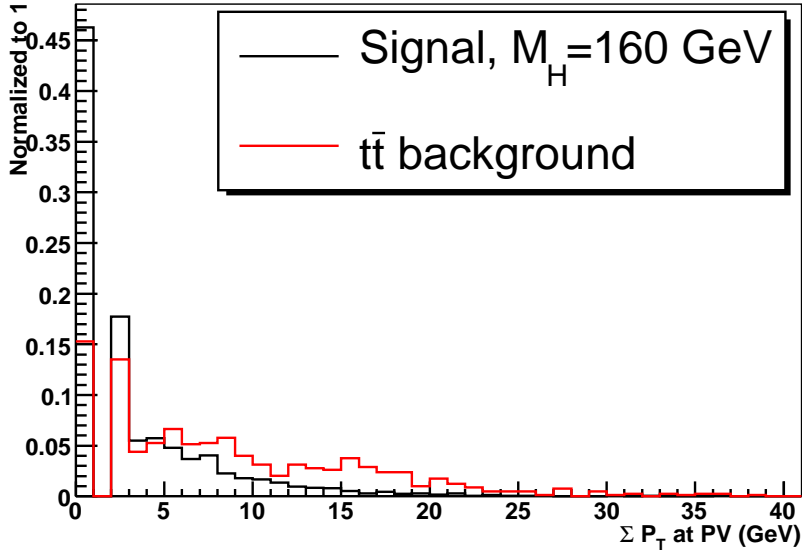


Figure 13: The scalar sum of the transverse momenta of all tracks (excluding the tracks from leptons) that point back to the primary vertex.

Cut	$gg \rightarrow H$ (fast)	$gg \rightarrow H$ (full)	$t\bar{t}$ (fast)	$t\bar{t}$ (full)
Trigger	246	254	9698	11776
P_T^{miss}	190	198	8143	9965
τ Rej.	185	193	7586	9303
Jet Veto	90.0	90.7	51.6	75.6
Vertex Veto	89.6	88.9	37.6	52.2
ΣS_0	89.6	85.9	37.6	37.2
ΣP_T	89.6	83.7	37.6	29.4
P_T^{Higgs}	53.2	48.5	33.0	24.5
M_{ll}	42.9	40.1	7.85	6.15
$\Delta\phi_{ll}$	33.1	30.6	5.23	4.05
M_T	31.2	29.6	3.64	2.89
Primary Control	2.10	1.50	33.4	25.53
b-tagged Control	0.10	0.26	17.02	25.86

Table 9: Cut flows (in fb) for $M_H = 160$ GeV in the $e\mu$ channel for fast and full simulation, and the cross-sections in the control samples (summed over lepton flavor).

Table 9 shows the cut flow in full simulation, with the corresponding numbers for fast simulation (taken from Table 1) shown again for convenience. The table also contains the cross-sections after all cuts for the Primary and b-tagged control samples. In the b-tagged control sample, we have required the presence of a displaced vertex with a displacement significance of at least 3σ , and no cuts are placed on the other Top-killing variables listed above. For the most part, the agreement is quite good; however, it would seem that the top background is not behaving quite the same way as it did in fast simulation. This is a serious concern, since an overestimate of the $t\bar{t}$ background in the control sample would imply an underestimate of the QCD WW background in the signal-like region and vice-versa. The difference is attributable to two effects:

- In the b-vetoed samples in full simulation, we apply a vertexing cut as well as two other tracking-based cuts, whereas in the b-tagged sample, we only apply a vertexing cut. By contrast, in the fast simulation, the distinction between the Primary control sample and the b-tagged control sample was based on (a parameterization of) a cut on a single b-tagging likelihood weight.
- In the fast simulation, our monte carlo sample for the $t\bar{t}$ background was generated by forcing both of the W bosons from top decay to decay leptonically. In the full simulation, on the other hand, we have allowed the W bosons to decay freely, and we have merely required that the Monte Carlo truth contain two leptons inside the range of tracking. Thus, our full simulation sample contains a contribution from events where only one W decays leptonically, and the second lepton in the event comes from the semileptonic decay of a b quark.

Isolation Criteria	Sample	$gg \rightarrow H$	$t\bar{t}$
0.2 (default)	Signal-like Region	32.2	5.59
	Primary Control	1.67	45.5
	b-tagged Control	0.27	25.9
0.2 (tight)	Signal-like Region	31.0	5.13
	Primary Control	1.60	40.8
	b-tagged Control	0.27	22.4
0.4	Signal-like Region	31.1	4.42
	Primary Control	1.60	35.0
	b-tagged Control	0.20	12.9
0.7	Signal-like Region	28.8	3.63
	Primary Control	1.48	27.0
	b-tagged Controls	0.12	8.15
Fast Sim.	Signal-like Region	31.2	3.64
	Primary Control	2.10	33.4
	b-tagged Control	0.10	17.0

Table 10: Cross-sections, in fb and based on full simulation, after all cuts (but excluding the $\text{Sum}(S_0)$ and $\text{Sum}(P_T)$ Top-killing cuts) for four different tunings of the lepton isolation cuts. The values obtained from fast simulation are shown for reference.

Table 10 shows the cross-sections in the signal-like region ($e\mu$ channel only) and the two control samples (summed over lepton flavor) using several slightly modified sets of lepton isolation cuts and ignoring the $\text{Sum}(P_T)$ and $\text{Sum}(S_0)$ isolation cuts. The four track isolation cut tunings we show are:

- the track isolation cuts we have used above, namely that the scalar $\text{Sum}(P_T)$ of tracks in a cone of 0.2 around the lepton be less than 10 GeV for electrons, or 5 GeV for muons;
- the same cone size, but tightening the cuts to 2 GeV for both electrons and muons;
- a widened cone of 0.4 units of R, with cuts of 5 GeV for electrons and 3 GeV for muons;
- a widened cone of 0.7 units of R, with cuts of 5 GeV for electrons and 3 GeV for muons.

It is clear from the table that the lepton isolation cuts can be tuned to reproduce the values of $\alpha_{t\bar{t}}$ and $\alpha_{t\bar{t}}^{WW}$ assumed in fast simulation. In Section 5.1, we will briefly propose a potential strategy to measure the performance of the Top-killing cuts, but we postpone an investigation of how to measure the efficiency of the lepton isolation cuts (and their power to reject $t\bar{t}$ in events with the configuration studied here) using data until a future study.

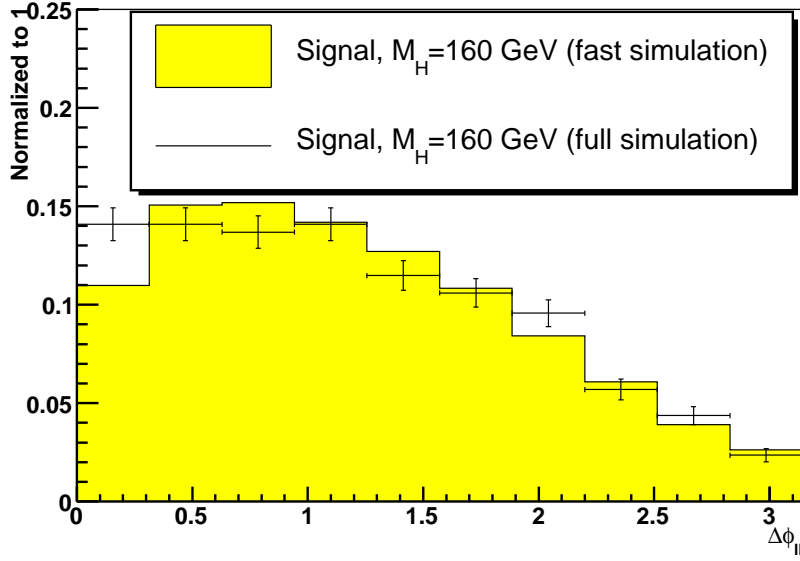


Figure 14: The distribution of the dilepton opening angle in signal using fast and full simulation. The error bars represent statistical errors due to the finite size of our Monte Carlo sample.

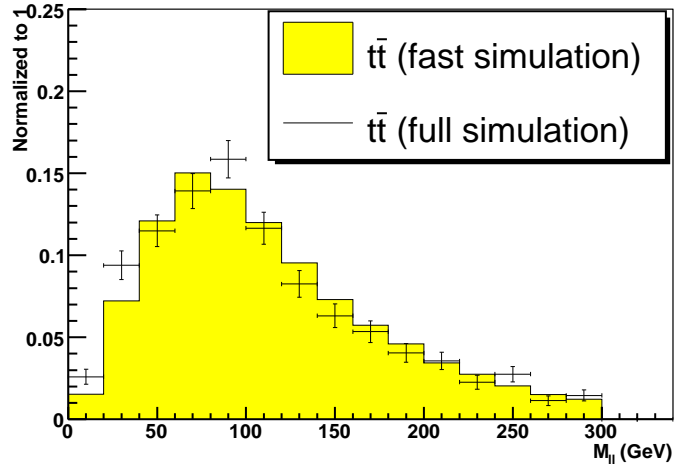


Figure 15: The distribution of the dilepton invariant mass in the $t\bar{t}$ background using fast and full simulation. The error bars represent statistical errors due to the finite size of our Monte Carlo sample.

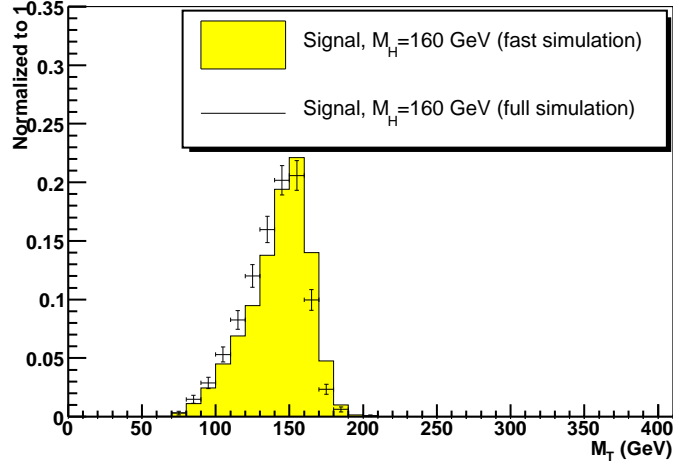


Figure 16: The distribution of the transverse mass in signal using fast and full simulation. The error bars represent statistical errors due to the finite size of our Monte Carlo sample.

Before we proceed, however, it is worthwhile to check that the fast and full simulation agree on the distributions of variables important to the analysis. Figure 14 shows the dilepton opening angle in the transverse plane. The small discrepancy at small $\Delta\phi_{ll}$ is most likely related to the lepton isolation, which we have already shown is in need of further study. Figure 15 shows the dilepton invariant mass in the $t\bar{t}$ background. Although the statistics are poor, the agreement is nonetheless satisfactory. Lastly, Figure 16 shows the transverse mass distribution for the signal. There appears to be a slight shift in the location of the peak, but the shift, if it is a real effect and not due to statistics, is miniscule compared to the broad mass window we apply.

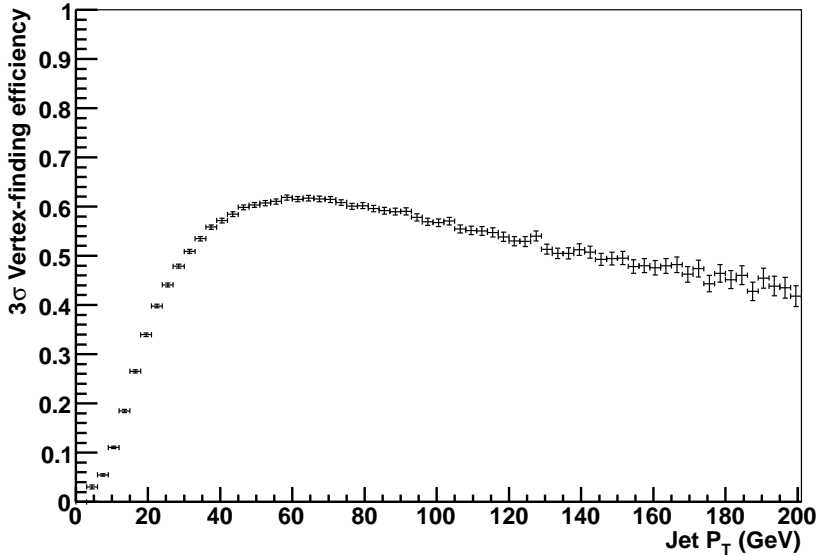


Figure 17: The probability to find a 3σ displaced vertex in a truth-matched b-jet as a function of the observed P_T .

5.1 Control Samples for Top Rejection

In this section, we propose an approach to estimate the efficiency of our Top-killing cuts in data. Here, we only outline the basic idea; a more detailed study of the systematics of this method will be the subject of future study.

There are three cuts we aim to understand here: the cut on the vertex displacement, the cut on the scalar $\text{Sum}(P_T)$ of tracks near the primary vertex, and the cut on the $\text{Sum}(S_0)$ of tracks in either of the two leading jets. We begin with the first of these three, since it is the most important.

A critical observation here is that the probability to find a 3σ displaced vertex in a truth-matched b-jet is a strong function of the P_T of the jet in the region below the jet veto threshold. Figure 17 shows the probability to find a displaced vertex in a truth-matched b-jet as a function of the P_T of the b-jet. (Note that no b-jet specific calibration has been applied to the jets here.) Our analysis takes place entirely in this region; any event with a jet above the jet veto threshold will be rejected.

Because the vertex-finding efficiency is such a strong function of the jet P_T in this region, only the hardest b-quark with $|\eta| < 2.5$ has a significant chance of giving an observable displaced vertex. The other b-quark must have a lower P_T , or it must be outside of tracking; therefore, the probability to find a displaced vertex in the corresponding jet is significantly smaller. This argument is further strengthened by a quick

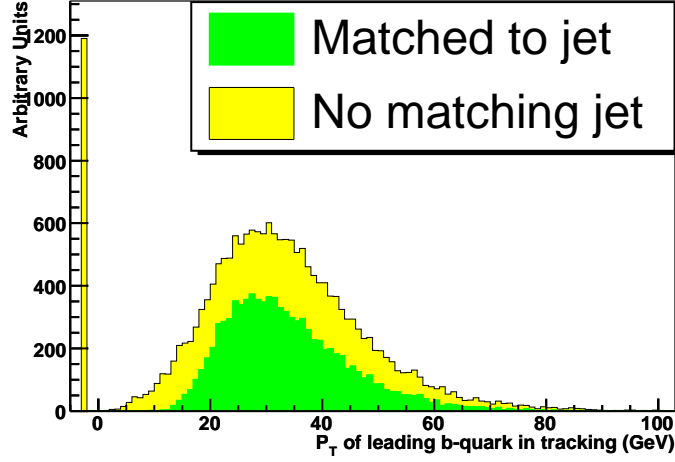


Figure 18: The P_T distribution of the highest- P_T true b-quark that lies in the region $|\eta| < 2.5$ in leading-order (i.e., MadEvent) doubly-resonant top events. The green region corresponds to b-quarks that are within a cone of 0.4 units of R around a reconstructed (ATLFAST) jet. The spike at 0 corresponds to events where there is no b-quark with $|\eta| < 2.5$.

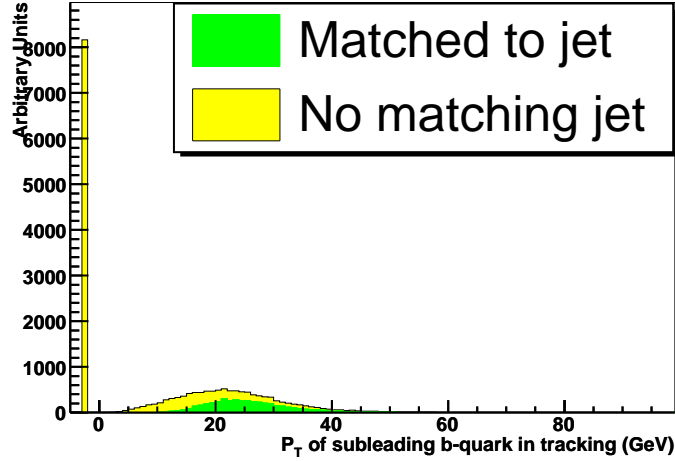


Figure 19: The P_T distribution of the second highest- P_T true b-quark that lies in the region $|\eta| < 2.5$ in leading-order (i.e., MadEvent) doubly-resonant top events. The green region corresponds to b-quarks that are within a cone of 0.4 units of R around a reconstructed (ATLFAST) jet. The spike at 0 corresponds to events where there is only one b-quark with $|\eta| < 2.5$.

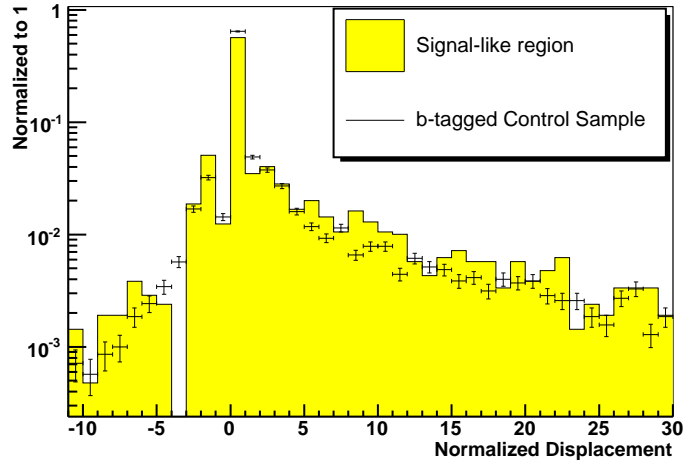


Figure 20: The normalized displacement of the most displaced vertex in the signal-like region (yellow) and most displaced vertex outside the leading (b-tagged) jet in the control sample defined by the presence of a hard, b-tagged jet (black). The error bars represent the statistical error due to the finite size of our Monte Carlo sample.

look at the Monte Carlo truth. Figures 18 and 19 (based on doubly-resonant top events generated with MadEvent) show the P_T distribution of the hardest (true) b-quark in $|\eta| < 2.5$ and the second-hardest (true) b-quark in the same region, respectively. The spike at zero indicates the fraction of events where either one or both of the b-quarks in the Monte Carlo truth are outside the range of tracking or are not matched to an observed ATLFASST jet. Clearly, there are very few events after the jet veto where both of the true b-quarks in the event are matched to an observed jet in tracking.

With that in mind, our approach for measuring the vertex-finding efficiency in the jet-vetoed region is to use a control sample that contains exactly one hard, b-tagged jet. (To be more specific: we use the same cuts that we used in the b-tagged control sample, but we require the existence of exactly one jet with transverse momentum larger than the jet veto threshold and vertex displacement larger than 3σ .) Obviously, this selection will give us a sample of highly top-enriched events; we therefore know that there must be another b-quark *somewhere* in the event, even if that b-quark is outside of tracking. Figure 20 shows the distribution of the displacement of the most displaced vertex in the event in the fully jet vetoed region compared to the distribution of the displacement of the most displaced vertex outside the leading jet in the hard b-tagged control sample. There is a small but clear bias in the result.

To understand the bias, it helps to know what is happening at the parton level. Because the leading jet is now required to be a b-tagged jet with $P_T > 20$ GeV, the kinematics of the subleading b-quark in this control sample resemble (to some extent)

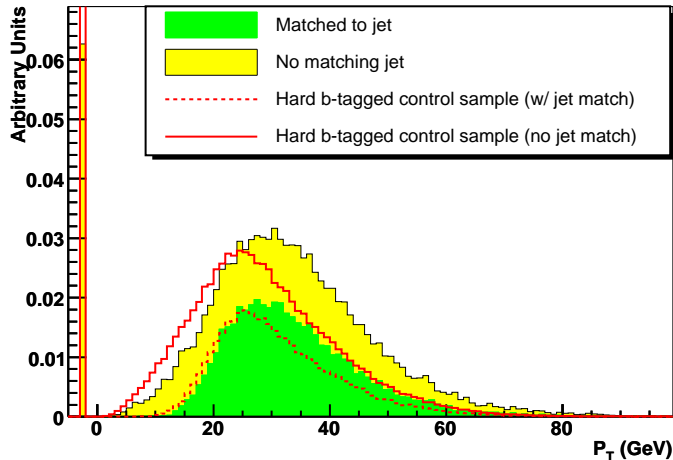


Figure 21: The P_T distribution of the highest- P_T true b -quark that lies in the region $|\eta| < 2.5$ in leading-order (i.e., MadEvent) doubly-resonant top events. The red curves show the same distributions for the subleading b -quark in the control sample defined by the presence of a hard, b -tagged jet.

the kinematics of the leading b -quark in the fully jet-vetoed region. Figure 21 shows a comparison between the P_T spectrum of the leading (true) b -quark in the fully jet-vetoed region and that of the subleading (true) b -quark in the region with one (b -tagged) jet above the jet veto threshold. The figure shows that although the kinematic distributions of the b -quarks in question are similar, the P_T spectrum of the b -quark is slightly harder in the fully jet-vetoed region than it is in the hard b -tagged sample. This explains the bias we observed in Figure 20: in the fully jet vetoed region, the fact that *both* b -jets are required to be below the jet veto threshold causes the average P_T of the leading b -quark in $|\eta| < 2.5$ to be slightly higher than the average P_T of the subleading b -quark in the hard b -tagged sample. The bias we saw above is primarily due to the configuration of phase space; it therefore makes sense to think that we can accurately account for it by applying a correction derived either from Monte Carlo or from some other calculation. The details of how to perform such a computation are beyond the scope of this feasibility study, although it is obvious that the exact method for deriving any such correction should be explicitly set forth before data-taking begins.

We skip over the second variable in our simple Top-killing algorithm for the moment, and instead turn our attention to the third variable, the scalar $\text{Sum}(P_T)$ of tracks that point back to the primary vertex. The physics motivation for this cut is the high Q^2 of top quark events; such events are generally expected to have more hadronic activity than the signal or the QCD WW background. In principle, the $\text{Sum}(P_T)$ cut should therefore be uncorrelated to cuts on the vertex displacement, since the underlying physics that gives rise to displaced vertices is the lifetime of the B meson.

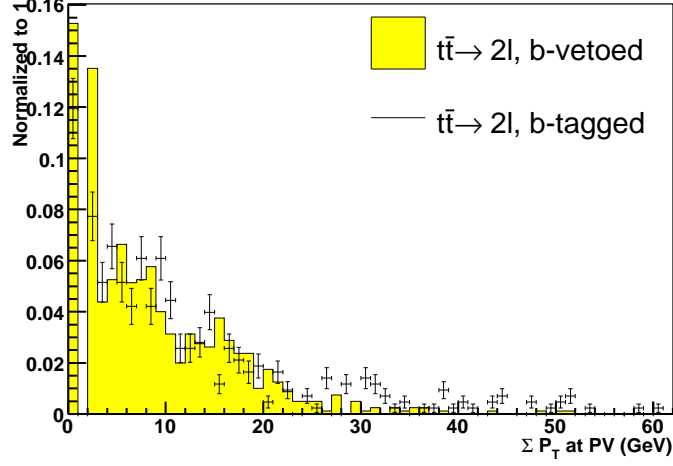


Figure 22: The distribution of the scalar $\text{Sum}(P_T)$ of tracks that point back to the primary vertex in the signal-like region and the (fully vetoed) b-tagged control sample. The error bars represent statistical errors due to the finite size of our Monte Carlo sample.

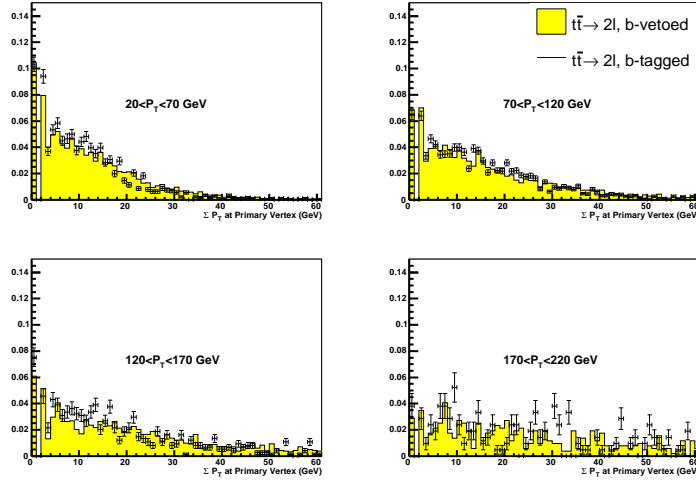


Figure 23: The scalar $\text{Sum}(P_T)$ of tracks that point to the primary vertex in events with exactly one hard jet with $P_T > 20$, in bins of the P_T of the hard jet. The yellow region represents events with a veto on displaced vertices; the crosses represent events that have a displaced vertex. The error bars indicate statistical errors due to the finite size of our Monte Carlo sample.

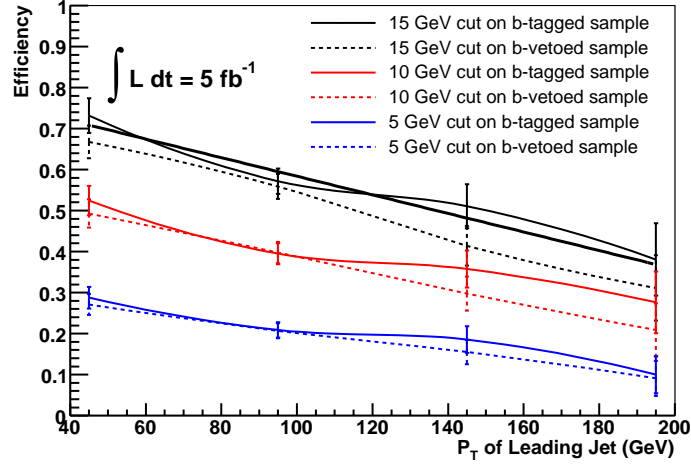


Figure 24: The efficiency (as a function of the P_T of the leading jet in the event) of three different cuts on the scalar $\text{Sum}(P_T)$ of tracks that point back to the primary vertex for events with a displaced vertex tag (solid lines) and a displaced vertex veto (dashed lines). Here, only the $t\bar{t}$ process is used to calculate these efficiencies.

Cut (GeV)	Target Value	Extrapolated
5	0.38423	0.31720
10	0.65207	0.55800
15	0.78849	0.78841

Table 11: For three different values of a cut on the $\text{Sum}(P_T)$ of tracks that point back to the primary vertex: the efficiency of the cut in the signal-like region (Target Value) and the efficiency as measured by extrapolating from the hard b-tagged control sample.

Consequently, one would expect that we could (in principle) simply plot the $\text{Sum}(P_T)$ distribution in the b-tagged, fully jet vetoed control sample and expect it to be the same as in the b-vetoed, fully jet vetoed control sample. Figure 22 shows that the shape of this variable is similar in the signal-like region and the control sample, but with a small bias that is probably due to the rapidly changing vertex-finding efficiency in the fully jet-vetoed region. Because of this, and because the cross-section in this region is too small to make an accurate measurement of the efficiency of the $\text{Sum}(P_T)$ cut, we do not regard this approach as the most practical one. Instead, we again look to the hard b-tagged control sample; Figure 23 shows a comparison of the $\text{Sum}(P_T)$ distribution for top events in b-tagged and b-vetoed configurations in bins of the P_T of the hard b-tagged jet. The agreement between the distributions is good in each bin (although we obviously cannot check this agreement in data because the b-vetoed sample would be heavily contaminated by QCD $WW + jets$ events). Figure 24 shows the efficiency of three possible cuts on the $\text{Sum}(P_T)$ as a function of the P_T of the leading jet, based on the binning in Figure 23. In practice, one would measure the efficiency of a given value of the $\text{Sum}(P_T)$ cut as a function of the leading jet P_T , fit the measured efficiencies, and extrapolate back to the signal-like region with leading jet $P_T < 20\text{GeV}$. For this exercise, we use the four bins shown in Figure 23, fit the efficiencies to a linear function, and take the extrapolated value in the signal-like region to be the value of the fitted function for a P_T of 10 GeV. The results are shown in Table 11. The table suggests that we can obtain a reasonable estimate of the efficiency of the $\text{Sum}(P_T)$ cut by extrapolating from the hard b-tagged sample to the fully jet-vetoed sample; in the near future, we intend to provide an updated version of this note which will make this argument using better Monte Carlo statistics.

Ideally, we would like to employ a similar extrapolation procedure to understand the $\text{Sum}(S_0)$ distribution as well, but it is obvious that an unbiased measurement is not easy with the control samples we have considered here. In a future work, we may attempt to devise a technique to control this cut using data. However, since this analysis can clearly function quite well without the $\text{Sum}(S_0)$ cut, we will not attempt such an undertaking here.

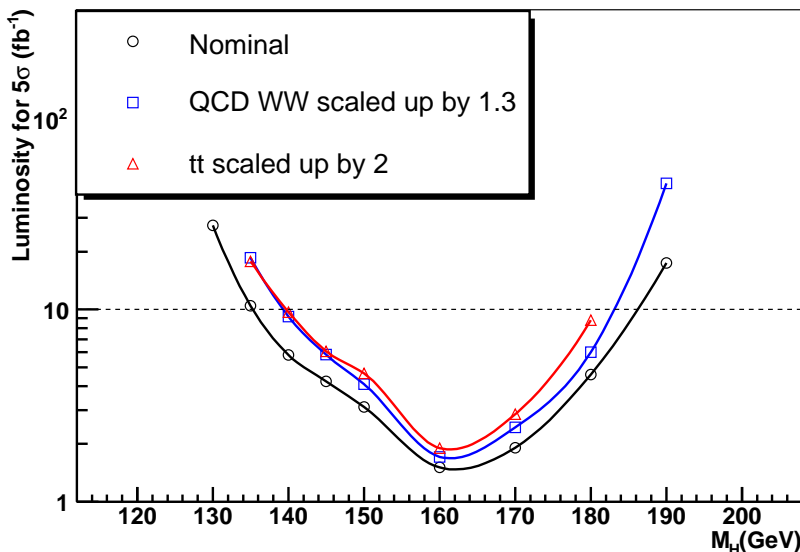


Figure 25: The luminosity required to reach a 5σ discovery for Higgs masses between 115 and 500 GeV. The black curve with circles shows the result using the cross-sections assumed throughout this note. The blue (squares) curve shows the corresponding results assuming that the cross-sections for all components of the QCD WW background are scaled up by 30% in the signal-like region and the control samples, and the red (triangles) curve shows the result obtained if the top background is doubled.

6 Sensitivity

In this subsection, we discuss the sensitivity of the analysis. We choose to express our result as the luminosity required to reach a 5σ discovery⁹; this quantity is shown as a function of the Higgs mass in Figure 25. Here, we have computed luminosity-dependent systematic errors on the normalization of the QCD WW and $t\bar{t}$ backgrounds using the control samples presented in Section 4 and taken the uncertainties on the other backgrounds to be 10% each. (This result is based entirely on fast simulation.) In the figure, we show three curves. The black curve (circles) is the luminosity required for discovery assuming the background cross-sections used throughout this note; the blue curve (squares) assumes the overall normalization of the QCD WW background is increased by 30%; and the red curve (triangles) shows the corresponding result if the top background is taken to be a factor of 2 larger than we have assumed here.

⁹That is, the luminosity required to have a 50% or greater probability to make a 5σ discovery.

7 Summary

We have investigated the sensitivity of a search for Higgs decays to W pairs in events where the Higgs is produced in association with no hard jets. Our approach explicitly defines control samples to determine the normalization of the QCD WW and $t\bar{t}$ backgrounds, and we have investigated the systematic errors on this background determination strategy. To our knowledge, this is the first study to address in detail the crucial issue of systematic errors on the background determination in this difficult number-counting analysis. We have studied this channel in full simulation, and shown that the performance assumed in fast simulation is reasonable. We conclude that the channel $H + 0j$ with $H \rightarrow WW \rightarrow l\nu l\nu$ is very robust and has a strong potential for an early Higgs discovery across a broad mass range.

8 Acknowledgement

The authors are grateful to N. Kauer, S. Frixione, M. Mangano, F. Krauss, and the Sherpa team. This work was supported in part by the United States Department of Energy through Grant No. DE-FG0295-ER40896.

References

- [1] F. Englert, R. Brout, Phys. Rev. Lett. **13** (1964) 321.
- [2] P. W. Higgs, Phys. Lett. **12** (1964) 132.
- [3] P. W. Higgs, Phys. Rev. Lett. **13** (1964) 508.
- [4] P. W. Higgs, Phys. Rev. **145** (1966) 1156.
- [5] G. S. Guralnik, C. R. Hagen and T. W. B. Kibble, Phys. Rev. Lett. **13** (1964) 585.
- [6] T. W. B. Kibble, Phys. Rev. **155** (1967) 1554.
- [7] M. Dittmar and H. Dreiner, Phys. Rev. **D55** (1997) 167.
- [8] ATLAS Collaboration, ATLAS Detector and Physics Performance, CERN/LHCC 99-15 (1999).
- [9] S. Frixione and B.R. Webber, JHEP **0206** (2002) 029.
- [10] S. Frixione, P. Nason and B.R. Webber, JHEP **0308** (2003) 007.
- [11] T. Gleisberg, S. Hoeche, F. Krauss, A. Schaelicke, S. Schumann, J. Winter, JHEP **0402** (2004) 056.

- [12] M.L. Mangano, M. Moretti, F. Piccinini, R. Pittau, A. Polosa, *JHEP* **0307** (2003) 001.
- [13] M.L. Mangano, M. Moretti, R. Pittau, *Nucl.Phys.B* **632** (2002) 343–362.
- [14] F. Caravaglios, M. L. Mangano, M. Moretti, R. Pittau, *Nucl.Phys.B* **539** (1999) 215–232.
- [15] B. Mellado, G. Unal, Sau Lan Wu, SM Higgs Production Cross-Sections and Branching Ratios for the ATLAS Higgs Working Group, ATLAS internal note ATL-COM-PHYS-2004-062.
- [16] K. Cranmer, Y. Fang, B Mellado, S. Paganis, W. Quayle, Sau Lan Wu, Analysis of VBF $H \rightarrow WW \rightarrow \nu\nu$, ATLAS Internal Note ATL-PHYS-2004-019.
- [17] Torbjörn Sjöstrand, High-Energy Physics Event Generation with PYTHIA 5.7 and JETSET 7.4, *Comp. Phys. Comm.* **82** (1994) 74.
- [18] Torbjörn Sjöstrand et al., High-Energy-Physics Event Generation with PYTHIA 6.1, *Comp. Phys. Comm.* **135** (2001) 238.
- [19] T. Binoth, M. Ciccolini, N. Kauer, M. Krämer, *JHEP* **0503** (2005) 065.
- [20] M. Dührssen, K. Jakobs, P. Marquard, J. J. van der Bij, *JHEP* **0505** (2005) 064.
- [21] F.Maltoni and T. Stelzer, hep-ph/0208156.
- [22] T. Stelzer and W.F. Long, *Phys. Commun.* **81** (1994) 357–371.
- [23] H. Murayama, I. Watanabe, and K. Hagiwara, *HELAS Manual*, 1991.
- [24] E. Richter-Was, D. Froidevaux and L. Poggioli, ATLFAST2.0 a Fast Simulation Package for ATLAS, ATLAS Internal Note ATL-PHYS-98-131.
- [25] S. Catani, F. Krauss, R. Kuhn, B.R. Webber, *JHEP* **0111** (2001) 063.
- [26] S. Correard, V. Kostyukhine, J. Leveque, A. Rozanov, J. B. de Vivie de Regie, b-tagging with DC1 data, ATLAS internal note ATL-PHYS-2004-006.
- [27] J. Pumplin, D.R. Stump, J. Huston, H.L. Lai, P. Nadolsky, W.K. Tung, *JHEP* **0207** (2002) 012.
- [28] Z. Bern et al., *Phys. Rev. D* **66** (2002) 074018.
- [29] A. Belyaev, E. Boos, *Phys. Rev. D* **63** (2001) 034012.
- [30] N. Kauer, D. Zeppenfeld, *Phys. Rev. D* **65** (2001) 014021.
- [31] Y. Fang, B. Mellado, S. Padhi, Sau Lan Wu, Object-based approach for the Reconstruction of Missing Transverse Momentum with the ATLAS detector, ATLAS internal note, in preparation.

- [32] V. Kostyukhine, VKalVrt - package for vertex reconstruction in ATLAS, ATLAS internal note ATL-PHYS-2003-031.
- [33] V. Kostyukhine, Secondary vertex based b-tagging, ATLAS internal note ATL-PHYS-2003-033.

M_H	$gg \rightarrow H$	VBF	$t\bar{t}$	EW WW	$gg \rightarrow WW$	$qq \rightarrow WW$	$\tau\tau$	ee
120	0.90	0.02	0.43	0.002	0.38	6.43	0.004	0.68
125	1.56	0.03	0.56	0.002	0.49	7.50	0.004	0.85
130	2.47	0.05	0.64	0.002	0.61	8.59	0.004	0.85
135	3.45	0.08	0.80	0.003	0.74	9.68	0.004	0.51
140	4.65	0.12	0.97	0.003	0.89	10.7	0.004	0.68
145	5.92	0.16	1.14	0.004	1.04	11.6	0.004	0.68
150	7.22	0.20	1.31	0.005	1.19	12.3	0.004	1.02
160	11.2	0.34	1.63	0.005	1.46	13.3	0.007	1.53
170	10.2	0.34	1.89	0.006	1.66	13.8	0.004	1.70
180	7.32	0.27	2.09	0.007	1.77	13.6	0.004	1.70
190	4.61	0.18	2.29	0.009	1.80	13.0	0.004	1.36
200	3.24	0.14	2.34	0.009	1.76	12.1	0.004	1.87

Table 12: Cross-sections (in fb) in the $e - e$ channel after the cuts in Section 3. Higgs masses are in GeV.

A Supplementary Tables

In this section we collect several tables that are worth documenting, but do not fit well in the main body of the text.

M_H	$gg \rightarrow H$	VBF	$t\bar{t}$	EW WW	$gg \rightarrow WW$	$qq \rightarrow WW$	$\tau\tau$
120	3.43	0.07	1.40	0.002	1.28	23.5	0.03
125	5.46	0.12	1.62	0.003	1.53	25.8	0.03
130	7.97	0.19	1.88	0.004	1.80	28.0	0.03
135	10.7	0.27	2.19	0.005	2.10	30.1	0.03
140	13.6	0.36	2.51	0.006	2.42	32.0	0.04
145	16.4	0.44	2.77	0.006	2.74	33.8	0.05
150	19.3	0.56	3.06	0.007	3.06	35.1	0.06
160	27.6	0.86	3.64	0.008	3.61	36.8	0.06
170	24.7	0.81	4.17	0.012	3.99	36.9	0.05
180	17.6	0.63	4.57	0.015	4.18	35.9	0.06
190	10.7	0.42	5.01	0.015	4.23	34.2	0.05
200	7.55	0.32	5.24	0.016	4.16	32.0	0.06

Table 13: Cross-sections (in fb) in the $e - \mu$ channel after the cuts in Section 3. Higgs masses are in GeV.

M_H	$gg \rightarrow H$	VBF	$t\bar{t}$	EW WW	$gg \rightarrow WW$	$qq \rightarrow WW$	$\tau\tau$	$\mu\mu$
120	0.92	0.02	0.24	0.001	0.34	6.20	0.01	0.00
125	1.56	0.03	0.32	0.002	0.44	7.25	0.01	0.37
130	2.46	0.05	0.37	0.002	0.56	8.38	0.01	0.18
135	3.45	0.08	0.46	0.002	0.68	9.48	0.01	0.37
140	4.62	0.12	0.53	0.002	0.82	10.4	0.01	0.37
145	5.81	0.16	0.71	0.002	0.97	11.3	0.01	0.73
150	7.10	0.20	0.81	0.003	1.11	12.0	0.01	0.73
160	11.0	0.33	1.04	0.004	1.38	13.0	0.01	0.73
170	9.88	0.33	1.19	0.004	1.57	13.4	0.01	0.55
180	7.10	0.25	1.41	0.004	1.69	13.3	0.01	0.91
190	4.45	0.18	1.60	0.004	1.72	12.7	0.01	0.91
200	3.14	0.13	1.67	0.004	1.70	11.9	0.01	0.73

Table 14: Cross-sections (in fb) in the $\mu - \mu$ channel after the cuts in Section 3. Higgs masses are in GeV.

M_H	$gg \rightarrow H$	VBF	$t\bar{t}$	EW WW	$gg \rightarrow WW$	$qq \rightarrow WW$	$Z \rightarrow X$
120	-	-	36.6	0.10	7.87	177.5	10.3
125	0.03	-	36.1	0.10	7.66	169.1	9.68
130	0.14	-	35.8	0.10	7.45	161.0	10.2
135	0.37	0.01	35.4	0.10	7.23	153.4	9.19
140	0.71	0.01	35.0	0.09	7.03	146.3	9.35
145	1.16	0.02	34.9	0.09	6.82	139.4	9.02
150	1.65	0.03	34.3	0.09	6.60	133.0	8.50
160	1.86	0.03	33.4	0.08	6.19	121.0	7.96
170	3.51	0.06	32.5	0.08	5.80	110.0	6.71
180	6.17	0.13	31.7	0.07	5.41	99.8	7.07
190	7.09	0.18	30.7	0.07	5.04	90.2	6.56
200	8.03	0.24	29.7	0.06	4.67	81.4	5.65

Table 15: Cross-sections (in fb, summed over lepton flavor) in the main (i.e. not b-tagged) control sample discussed in Section 4. Higgs masses are in GeV. A “-” denotes a value less than 0.01.

M_H	$gg \rightarrow H$	VBF	$t\bar{t}$	EW WW	QCD WW	$Z \rightarrow X$	
120	0.02	-	18.0	-	0.08	1.66	1.16
125	0.04	-	17.9	-	0.08	1.60	1.22
130	0.06	-	17.6	-	0.08	1.65	1.06
135	0.07	-	17.6	-	0.08	1.63	1.06
140	0.11	-	17.6	-	0.08	1.62	0.87
145	0.14	-	17.3	-	0.07	1.59	0.84
150	0.16	0.01	17.2	-	0.08	1.56	1.16
160	0.18	0.01	17.0	-	0.08	1.51	1.29
170	0.17	0.01	16.7	-	0.07	1.49	1.67
180	0.17	0.01	16.2	-	0.07	1.38	1.09
190	0.14	0.01	15.9	-	0.06	1.38	1.39
200	0.13	0.01	15.4	-	0.06	1.29	1.10

Table 16: Cross-sections (in fb, summed over lepton flavor) in the b-tagged control sample discussed in Section 4. Higgs masses are in GeV. A “-” denotes a value less than 0.1.